J. Membrane Biol. 203, 83–99 (2005)
DOI: 10.1007/s00232-005-0734-y

The Journal of
Membrane
Biology

A Subsequent Fit of Time Series and Amplitude Histogram of Patch-Clamp Records Reveals Rate Constants up to 1 per Microsecond

I. Schröder, P. Harlfinger, T. Huth, U.P. Hansen
Center of Biochemistry and Molecular Biology, Leibnizstr. 11, 24098, Kiel, Germany

Received: 20 September 2004/Revised: 5 January 2004

Abstract. Fast gating in time series of patch-clamp current demands powerful tools to reveal the rate constants of the adequate Hidden Markov model. Here, two approaches are presented to improve the temporal resolution of the direct fit of the time series. First, the prediction algorithm is extended to include intermediate currents between the nominal levels as caused by the anti-aliasing filter. This approach can reveal rate constants that are about 4 times higher than the corner frequency of the anti-aliasing filter. However, this approach is restricted to time series with very low noise. Second, the direct fit of the time series is combined with a beta fit, i.e., a fit of the deviations of the amplitude histogram from the Gaussian distribution. Since the ''theoretical'' amplitude histograms for higher-order Bessel filters cannot be calculated by analytical tools, they are generated from simulated time series. In a first approach, a simultaneous fit of the time series and of the Beta fit is tested. This simultaneous fit, however, inherits the drawbacks of both approaches, not the benefits. More successful is a subsequent fit: The fit of the time series yields a set of rate constants. The subsequent Beta fit uses the slow rate constants of the fit of the time series as fixed parameters and the optimization algorithm is restricted to the fast ones. The efficiency of this approach is illustrated by means of time series obtained from simulation and from the dominant K^+ channel in *Chara*. This shows that temporal resolution can reach the microsecond range.

Key words: Anti-aliasing filter — Beta distributions — Hidden Markov models — Ion channels — Rate constants — Maximum likelihood

Introduction

Ion channels are not rigid cylinders that facilitate a steady stream of ions across biological membranes. Instead, they are vibrating proteins leading to spontaneous or agent-induced interruptions of the stream. The resulting closures and openings are modelled by means of Markov models (Korn & Horn, 1988; Yeo et al., 1988; Ball & Rice, 1992; Blunck et al., 1998). The rate constants of the transitions between the states of the Markov model even in a single channel span a wide range from about 1 s^{-1} to at least 1 μs^{-1} (Schröder et al., 2004). The upper limit is not known, because the temporal resolution of classical evaluation algorithms leads to a limit which is about 100,000 s^{-1} (Parzefall et al., 1998; Farokhi et al., 2000; Zheng et al., 2001; Hansen et al., 2003).

The different approaches commonly employed for the evaluation of patch-clamp time series offer different potencies for the analysis of fast gating. Widely applied is dwell-time analysis (Blunck et al. 1998). In order to account for fast gating, missed-events corrections have been suggested (Ball et al., 1993; Draber & Schultze, 1994). However, Farokhi et al. (2000) have found a horizontal dependence of the evaluated rate-constants on the ''true'' rate constants, which is not the optimum condition for correction algorithms. Dwell time analysis can become powerful if 2-dimensional histograms are evaluated (Magleby & Weiss, 1990).

The Beta fit is based on the generation of amplitude histograms and fitting their deviations from Gaussians by beta distributions (FitzHugh, 1983; Yellen, 1984; Klieber & Gradmann, 1993; Riessner, 1998). However, this approach is restricted to 2-state Markov models.

Abbreviations: BF1, BF4, Beta fit with a Bessel filter of first or fourth order, respectively; EP fit, direct fit of the time series with extended prediction (including the filter response); *C*, *G*, *Z* closed states; HMM, Hidden Markov model; *A*, *O* open state, SNR, signal-to-noise ratio; SP fit, direct fit of the time series with simple prediction (single-step prediction); SQ fit, subsequent SP/BF4 Fit.

Correspondence to: U.P. Hansen; email: uphansen@zbm.uni-kiel.de

So far, the best results have been obtained with the prediction fit, which is a direct fit to the time series using a Maximum Likelihood estimator (Fredkin & Rice, 1992; Albertsen & Hansen, 1994; Klein, Timmer & Honerkamp, 1997). Even the classical prediction fit can work quite well with rate constants higher than the filter frequency (Farokhi et al., 2000; Hansen et al., 2003).

The most comprehensive approach is that of Venkataramanan et al. (1998a,b, 2000). The memory introduced by the filter response is included into the prediction equations by using so-called meta states. The ensemble of Markov states observed at time t is expanded to a Markov field comprising the states at t, t-1 to t-n with n being determined by the order of the filter. Filter order and thus the size of the Markov field was reduced by de-convolution of the time series with the inverse filter. Colored noise, open-channel noise and the effect of the filter on the noise are included into calculated amplitude distribution functions per meta state using an autoregressive (AR) filter. Furthermore, the drift of the base line can be incorporated according to Venkataramanan and Sigworth (2002). This general concept has been modified by other authors, mainly in order to shorten computing time. Qin et al. (2000) used a direct optimization approach, which yields the rate constants and not the transition probabilities (Fredkin & Rice 1992; Albertsen & Hansen 1994). This was achieved by replacing the Baum-Welch algorithms by a fit routine. Decreasing computing time was obtained by reducing the number of meta states by clustering states of equal conductance for single and multiple channel records. Fredkin & Rice (2001) achieved a tremendous acceleration of the computations by excluding unlikely meta states. Michalek et al. (2000) also excluded unlikely meta states. However, the replacement of the AR filter by an ARMA filter for the filter response increased computer time. This was compensated by using an approximated likelihood.

Nevertheless, the computing times are still very long. In our data from the dominant K^+ channel in *Chara*, we have 2 to 16×10^6 data points sampled at 200 kHz. Normally, we have at least two channels in a record, and each channel has to be modelled by 5 states (Farokhi et al. 2000, Hansen et al. 2003). This takes 4 to 32 h on a 2.5-GHz Athlon computer, still using the algorithms of Albertsen and Hansen (1994). In order to account for the filter without increasing computing time too much, we considered two approaches: First, we tried an approach (EP fit) that can be visualized as an extreme reduction of the method of Venkataramanan et al. (1998a,b, 2000). The introduction of the filter into the prediction algorithm of the direct fit of the time series was further simplified, and we did not consider the effect of the filter on the noise. Second, it is tested whether a combined evaluation based on the direct fit of the time series with simple prediction (SP fit) and on the analysis of amplitude histograms (Beta fit) can move the time resolution to faster rate constants. As described below, the Beta fit makes use of the observation that fast gating causes deviations from the Gaussian shape of the measured amplitude histograms.

Mathematical Tools

Illustration of the Problem

The problem (and chance) of high temporal resolution is illustrated in Fig. 1. In the theory of Markov processes applied to ion channel analysis, it is assumed that the noise-free signal immediately jumps from one state of conductivity to another. In a real experiment, the transition is soft as caused by the inevitable anti-aliasing filter. Figure 1 shows the response of a 4^{th}-order Bessel filter with the sampling frequency being four times the corner frequency of the filter. The smooth vertical line shows the true jump of the Markov process at $t/T = 0$. The filter output, presented by the smooth sigmoidal curve, gives a delayed response.

The dotted vertical line shows where a level detector would see the jump. This is also the location that is delivered by the classical prediction fit of the time series as the average expected time of the jump, because in 50% of the investigated events this intermediate level would be assigned to the lower level and in 50% to the higher level.

In Figure 1, the data points before the dotted line have a higher probability of being assigned to the lower level, and those behind the dotted line are presumably assigned to the upper level. The location of the detected level is delayed by two sampling periods. However, this is not of concern because the jump out of the level is delayed by the same interval, thus leaving the dwell time in the level unaffected.

The major problem that is caused by the filter results from the fact that the channel may switch back before the filter has reached the threshold in Fig. 1. Thus, short jumps may remain undetected. Jumping is a stochastic process, the rate constants related to a transition of the Markov model result in an exponential distribution of dwell times, with the average of these dwell times being the inverse of the rate-constant. If the short transitions are not detected then the average dwell time is moved to longer time constants and the apparent rate constant is slower than the original one.

Fitting Strategies

Two approaches provide the fundaments for the investigations here; the prediction fit and the Beta fit. The prediction fit uses a prediction equation (*see* Eq.

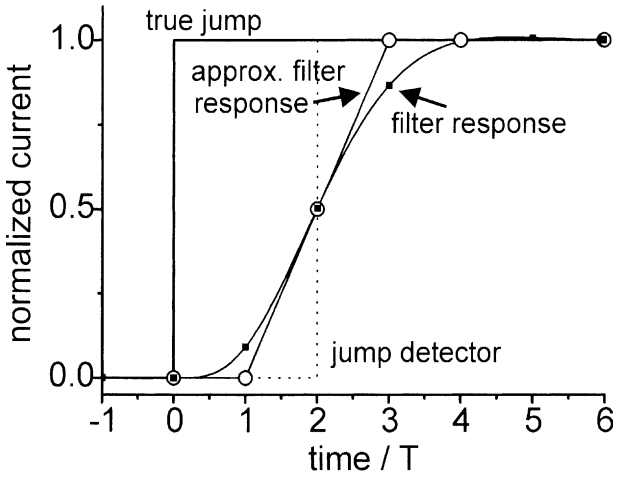

Fig. 1. Response of a 4-pole Bessel filter with a cut-off frequency of $4/T$ (T being the sampling interval) to a jump in noise-free channel current (smooth vertical line at time/$T=0$). The dots on the smooth sigmoidally increasing curve show the current values sampled at the output of the filter. The dotted vertical line indicates the jump as determined by a threshold jump detector. The straight increasing line (*empty circles*) presents the approximated response of the filter used in the fit with extended prediction (EP-fit) below.

3 below) in order to give an estimate of the Markov state at the next sampling point of the time series (Fredkin & Rice, 1992; Albertsen & Hansen, 1994; Klein, Timmer & Honerkamp, 1997; Farokhi et al., 2000; Hansen et al., 2003). It is also called a direct fit of the time series. The Beta fit utilizes the deviations of the measured amplitude histogram from that of a gaussian one (FitzHugh, 1983; Yellen, 1984; Klieber & Gradmann, 1993; Riessner, 1998).

All approaches discussed here are target fits. This implies that the fit seeks to provide results that are the target of our interest. In the case of Markov models, the rate constants are the natural parameters of modeling. If molecular dynamics are applied to channel gating, the rate constants, not the transition probabilities, are the experimental parameters suitable for testing the predictions of the model. This is different from some approaches such as dwell-time analysis, which normally yields amplitude factors and time constants of exponentials (Colqhoun et al., 1996). However, also dwell time analysis can be done as a target-fit (Kijima & Kijima, 1987; Blunck et al., 1998; Csanády 2000). Target fits avoid the cumbersome conversion of amplitude factors and time constants to rate constants (Jackson, 1997), but the evaluations depends on a priori knowledge (assumption) of the generating Markov model.

Markov Models

The gating of ion-channels can be described by Markov models (Korn & Horn, 1988), which consist of several states. These states may have different conductivities or different kinetic behavior. Adjacent states that cannot be distinguished by conductance or kinetic behavior can be merged into apparent states (Hansen Tittor & Gradman, 1983). Here, we use two different Markov models.

For investigations that are to illustrate basic insights or that are presented in order to show the failure of a suggested approach, a simple two-state model

$$C \underset{2q}{\overset{1q}{\rightleftharpoons}} O \tag{1}$$

is used. The factor q is changed in the range tests below. In order to show that a suggested approach works even under more complicated conditions, a 5-state model is used. It has been used by Farokhi et al. (2000) for the description of the gating of the dominant K^+ channel in *Chara*

$$A \underset{0.5}{\overset{1.5}{\rightleftharpoons}} O \underset{7q}{\overset{10q}{\rightleftharpoons}} G \underset{4}{\overset{3.5}{\rightleftharpoons}} C \underset{0.2}{\overset{0.5}{\rightleftharpoons}} Z \tag{2}$$

(rate constants in ms^{-1}). Its suitability as a model for testing algorithms arises from the feature that it comprises a wide spectrum of rate constants from very fast ones to very slow ones.

Curve-fitting

Below, different convergence criteria are employed: Maximum Likelihood for the direct fit of the time series and Least Square for the amplitude histogram. In either case, fitting is done under the guidance of a simplex algorithm (Caceci & Cacheris, 1984; Press et al. 1987). The generation of the start simplex is described in the Appendix. According to our experiments, in many fields of numerical evaluations of biological data, gradient-based methods mostly fail when the number of free parameters exceeds 2 or 3.

Failures of the fitting process can result from two causes: First, the convergence criterion may not have the correct dependence on the parameter sets. It can be too flat (as in the case of Beta distributions for slow rate constants) or it can even have its optimum value at the wrong parameter set (as in the case of the SP fit at high rate constants) and lead to the wrong solution. Second, the fitting algorithm (here the simplex) might not be able to find its way from the start simplex to the correct parameter set.

Here, simulated data are used to test the suggested evaluation algorithms. Thus, the true parameter values are a-priori known (in contrast to a real experiment). This facilitates two different approaches:

(*i*) Start simplex 1, including the correct parameter set ($\{s_{1,n}\} = \{k_{i,j}\}$ or $a = 1$ in Eq. A2). This is employed if it is to be shown that a fit algorithm fails, according to the statement "even if the correct value is known, the algorithm cannot reveal it from fitting the data".

(*ii*) Start simplex 2 excluding the correct parameter set. Using a start simplex that excludes the true values with $a \neq 1$ resembles the situation of a real experiment, where the true parameter set is not known. Then both features are tested: the existence of a correct convergence criterion and a smooth error landscape that opens a path to the correct parameter set.

New Approaches

First Improvement of the SP Fit: Extended Prediction Algorithm Accounting for the Slope of the Filter in the Prediction Algorithm

The classical SP fit has been discussed in detail by Fredkin & Rice (1992), Albertsen & Hansen (1994), Klein et al. (1997). More sophisticated approaches accounting for the filter response are mentioned in the introduction. Here, we test whether computer time can be reduced by a strong simplification of these approaches. The incorporation of meta states (Venkataramanan et al. 1998a,b, 2000) is replaced by a case differentiation in the prediction equation, and the effect of the filter on the noise is ignored. The filter response is approximated by the straight ascending slope in Fig. 1 marked by open circles. This approximation simplifies the prediction algorithm described below. It coincides with the true response at $t/T = 2$, but has minor deviations at $t/T = 1$ and $t/T = 3$. The improvement over the classical approach is the smaller deviation from the filter response (*filled squares*), as compared to the dotted line in Fig. 1, which is used in the simple prediction algorithm.

Again, the jump is realized too late (here it is only one sampling period). However, as mentioned above, the parallel shift of the times of the jumps into and out of a level does not change dwell times.

In the classical approach, which does not take the filter into account, the prediction (forward calculation) for the open state of a two-state *O*-*C* model is

$$a_k(O) = a_{k-1}(O)p_{OO}f_O(I_k) + a_{k-1}(C)p_{CO}f_O(I_k) \qquad (3)$$

with $a_j(B)$ being the probability of being in state B at time $t = jT$ ($j = k, k-1$), p_{AB} being the probability of a transition from state A to state B, $f_B(I_k)$ being the probability that the measured current I_k measured at time $t = kT$ can be assigned to the current of state B. The probability $f_B(I)$ is obtained by fitting the overall amplitude histogram by a sum of gaussians:

$$f(I) = \sum_B f_B(I) = \sum_B F_B \exp\left(\frac{(I - I_B)^2}{2\sigma_B^2}\right) \qquad (4)$$

Here, we assume that all σ_B are equal to σ, the noise of the jump-free time series. The scaling factors F_k are omitted, because the distributions per level are normalized to 1.

If a filter is involved, intermediate values of output current can occur. Figure 2 shows the four different scenarios, which describe the different ways from a closed into an open state at time k. The dotted lines in Figs. 2*B*, *C*, and *D* present the true jump occurring in channel current. As mentioned above, the approximation of the filter response by the straight slope in Fig. 1 results in the delay of the detected jump by one sampling period. For the sake of simplicity, this effect is ignored. Ignoring this delay has the effect that the solid vertical line in Fig. 2 presents the jump that is delivered by the evaluation algorithm.

The squares in Fig. 2 present the intermediate level Z resulting from the filter response in Fig. 1. The partial amplitude histogram related to the intermediate level Z is calculated from the noise of the jump-free time series with

$$f_Z(I_k) = \frac{1}{\sqrt{2\pi}\sigma}\exp\left(\frac{\left(I - \frac{1}{2}(I_p + I_a)\right)^2}{2\sigma^2}\right) \qquad (5)$$

with I_p and I_a being the levels before and after the jump, respectively.

From Figs. 2*A*, *B*, *C*, *D*, the extended prediction equation can be derived. The scenarios in Figs. 2*A*, *B*, *C*, *D*, correspond to the four terms in Eq. 6, respectively, as can easily be seen from a comparison of Eq. 6 with Fig. 2.

$$\begin{aligned} a_k(O) = {} & a_{k-1}(O)p_{OO} * [f_O(y_{k-1})f_O(y_k) + f_z(y_{k-1})f_O(y_k)] \\ & + a_{k-1}(C)p_{CO} * [f_O(y_{k-1})f_z(y_k) + f_z(y_{k-1})f_z(y_k)] \end{aligned} \qquad (6)$$

It is important to realize that only the probabilities a_k and a_{k-1} occur explicitly in Eq. 6, but not a_{k-2} at $t/T = k-2$. The probability a_{k-2}, however, is included in Eq. 6 by the differentiation of the four cases in Fig. 2.

Equations like Eq. 6 have to be set up for each one of the involved states of the Markov model. Further, the number of products in each equation increases with the number of states.

In the above equations, there is the inherent assumption that the jumps occur at the sampling points. This, of course, is not quite true. Nevertheless, the following analysis shows that Eq. 6 is already an improvement over the classical SP fit with the simple prediction in Eq. 3 (Albertsen & Hansen, 1994), but below it is shown that this holds only for very good SNR.

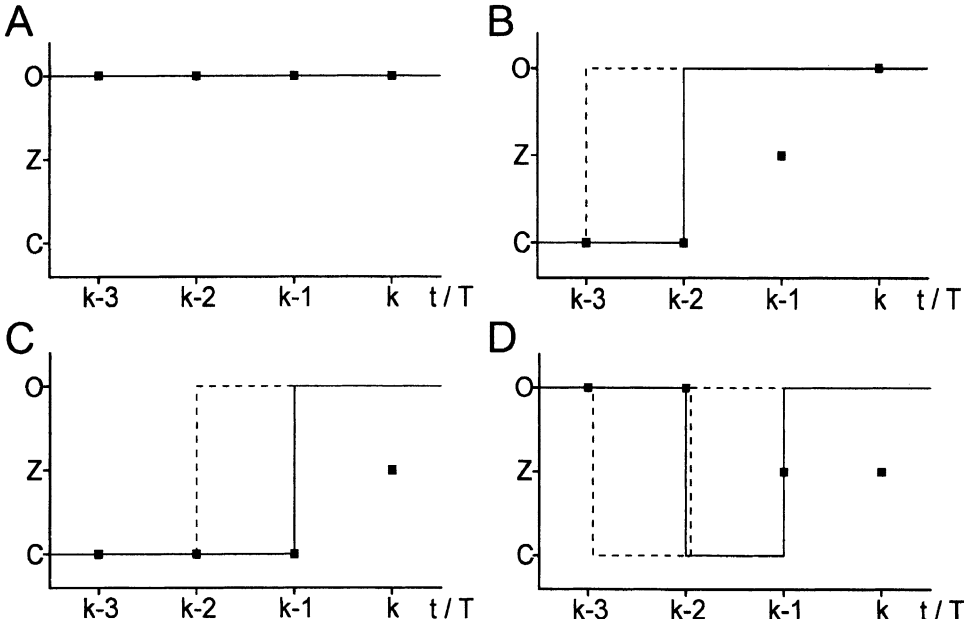

Fig. 2. Different scenarios which lead to an open state at time kT. The dotted lines show the true jumps of the Markov model. The continuous line presents the jump, which is delayed by one sampling period. This delayed jump is the input signal of a filter approximated by the straight ascending line in Fig. 1. The squares give the approximated sample output currents of the anti-aliasing filter (*empty circles* in Fig. 1). The four graphs show the filter response for different gating scenarios that would be detected if the prediction algorithm would work properly. This detected jump is delayed by one period as illustrated in Fig. 1. (*A*) No jump has occurred. All values remain at the same level. (*B*) A jump occurs at $t/T = k$-3. Then the channel is still at the initial level at $t/T = k$-2 and at the intermediate level Z at $t/T = k$-1. This scenario corresponds to Fig. 1. (*C*) The jump occurs at $t/T\,k$-2. Then $t/T = k$-2 and $t/T = k$-1 are still at the initial value. The intermediate value is reached a $t/T = k$. (*D*) A double jump has occurred Then, the initial value is measured still at $t/T = k$-2, and the values at $t/T = k$-1 and $t/T = k$ are at the intermediate level.

In order to determine the rate constants from a fitting routine the likelihood L is calculated

$$L = \prod_{k=1}^{N_S} \sum_{B}^{M} a_k(B) \tag{7}$$

with Ns being the number of all samples, B stands for all M states with $M = m^N$ of the macro-channel (Colquhoun & Hawkes, 1977, 1990; Blunck et al., 1998) representing N channels with m states. The value a_k is calculated iteratively from Eq. 3 or Eq. 6. The rate constants k_{AB} are related to the transition probabilities p_{AB} as follows (Albertsen & Hansen, 1994):

$$P = \exp(K \cdot T) \tag{8a}$$

with P and K being the matrices related to p_{AB} or k_{AB}, respectively. If the time interval is short with respect to k_{AB}, the relationship is simpler

$$p_{AB} = k_{AB} \cdot T \tag{8b}$$

The Simplex algorithm (*see* Appendix) employed in the fitting routine uses k_{AB} and calculates p_{AB}. Thus, Eq. 8*a* (or Eq. 8*b*) does not have to be inverted.

Multi-state Multi-channel Beta Distributions for Higher-Order Filters

Beta distributions (amplitude histograms) yield an alternative approach to evaluate fast rate constants from measured time series (FitzHugh, 1983; Yellen 1984; Klieber & Gradmann, 1993). So far, a general analysis has been restricted to two-state models. Riessner (1998) has developed an analytical algorithm to evaluate Hidden Markov models with more than two states and more than one channel. However, this analysis is restricted to first-order filters, which have little relevance in patch-clamp analysis. For two-state models, Yellen (1984) has suggested a correction factor to extend the first-order algorithms to higher-order filters. However, this has not worked in the case of multi-state models (probably also not in the case of two-state models, Riessner 1998).

Utilizing the increase of computer power since 1998, it became possible to use simulations for the "theoretical" amplitude histograms originating from higher-order filters and multi-state multi-channel models. For this issue, time series are generated by simulations as described in the Appendix, and the

amplitude histograms are generated by standard procedures.

Multi-channel amplitude distributions (A_N) are calculated iteratively by means of convolution

$$A_N(I) = \int A_1(u) \cdot A_{N-1}(I-u)du \tag{9}$$

with A_1 being a single-channel amplitude distribution and $A_{(N-1)}$ the distribution for $(N-1)$ channels. Also the amplitude distribution of noise W can be included by convolution

$$A(I) = \int A_N(u) \cdot W(I-u)du \tag{10}$$

In the case of gaussian noise, $W(u)$ can be calculated from the knowledge of the variance σ obtained from jump-free sections of the time series.

$$W(u) = \frac{1}{\sqrt{2\pi}\sigma} e^{-\frac{u^2}{2\sigma^2}} \tag{11}$$

In this approach, the spectral distribution of the noise is not important as long as the gaussian amplitude distribution is not distorted. Nevertheless, Eq. 10 offers also the possibility to include non-gaussian noise by replacing Eq. 11 by the adequate function.

Beta Fit

Fitting measured amplitude histograms to theoretical Beta distributions on the basis of an assumed Markov model minimizes

$$X^2 = \sum_{i=1}^{N_I} \frac{(A_{exp,i} - A_{theo,i})^2}{A_{exp,i} + 0.1} \tag{12}$$

$A_{exp,i}$ is a data point in the amplitude histogram obtained from the measured time series. $A_{theo,i}$ is a "theoretical" data point in the amplitude histogram generated by the time series simulated from an assumed Markov model as described above. N_I is the number of data points in the amplitude histograms (number of intervals on the current axis). The denominator prevents that the maximum values of the amplitude histogram get the highest weight. The highest values are close to Gaussian distribution, whereas the deviations carrying the information about fast gating are found at the slope of the distribution. The value 0.1 is added in order to prevent overflow resulting from division by zero.

The procedure is time-consuming as each step of the simplex algorithm requires one simulation of the time series. However, there is the advantage of Eqs. 9 and 10, which implies that multi-channel Beta distributions can be obtained from convolution of single-channel distributions. Thus, they do not require the time-consuming simulation of a macro-channel including the m^N states of an m-state N-channel scenario as in the SP fit of Albertsen & Hansen (1994).

The Simultaneous Fit of Beta Distributions and Time Series

Below it is shown that the fit of amplitude histograms (Beta fit) yields good results for high rate constants, whereas the direct fit of the time series (SP fit) gives better approximation for slow rate constants and is less sensitive to noise.

In order to merge both fits into one routine, the convergence criterion of the joint fit has to be a function of the convergence criteria of two individual fits. The SP fit maximizes the likelihood L (Eq. 7), whereas the Beta fit minimizes X^2 (Eq. 12). Thus, the sum of X^2 and the inverse of L are minimized

$$g \ln X^2 + \ln \frac{1}{L} \rightarrow Min \tag{13}$$

The logarithm of L is used because L becomes very small and this would lead to numerical problems in a computer if the product $1/L$ instead of the sum of $-\ln a_k$ (Eq. 7) would be calculated. This implies also the usage of $\ln X^2$, otherwise the error functions related to X^2 would be much steeper, and the effect of X^2 would override that of $\ln L$ in a fitting routine. Furthermore, there is a big difference in magnitude between $\ln X^2$ and $\ln L$. Thus, a weighting factor g is introduced. Factor $g = 0$ implies that the fit is completely based on the SP fit, whereas very high values of g (e.g., higher than 10^6) lead to the dominance of the Beta fit.

The Subsequent Simple Prediction/Beta Fit (SQ Fit)

Here, the direct fit of the time series with simple prediction (SP) and the Beta Fit with 4th order Bessel-Filter are not combined in parallel but subsequently: The robustness of the SP fit is used to give a first estimate of the rate constants. These results are used to generate a start simplex 1 for the Beta fit. Since the Beta fit has problems to determine slow rate constants, these rate constants are fixed during this second fitting step. This means that the simplex algorithm leaves the slow rate constants fixed at the values obtained from the SP fit and varies only the fast rate constants in order to fit the amplitude histogram. The threshold between "fast" and "slow" was set to ¼ of the filter frequency (12.5 ms^{-1}, in our investigations).

As final result, the slow rate constants from the SP Fit and the fast ones from the Beta Fit are taken.

Testing the Algorithms

Testing the algorithms is mainly based on two kinds of test. The range test is to investigate the temporal resolution. A set of about 250 (Figs. 3 and 4) or 50 (Figs. 5 and 8) time series is generated (*see* Appendix) with the pair of fast rate constants k_{ij} set to $q \cdot k_{ij,0}$, (Eqs. 1 or 2) with q being the number of the time series and $k_{ij,0}$ being the rate constants of the "slowest" time series. These time series are subject to the inspected algorithm, and it is determined up to which n the algorithm still yields the rate constants used in the simulation. The noise test deals with the sensitivity to noise. Time series having all the same rate constants k_{ij} are superimposed by noise of different strength. This yields the SNR (signal-to-noise ratio) down to which the true rate constants can be revealed by the algorithms.

Extended Prediction Fit Accounting for the Filter Response

For the investigations of what the direct fit of the time series with simple and extended prediction can do, a simple $C-O$ model is used, and the start simplex includes the true parameter set. In Fig. 3, the rate constants are about equal, namely $k_{OC} = q$ ms^{-1} and $k_{CO} = 2\ k_{OC}$ (with $q = 1$ to 250). The performance of the new approach is compared with that of the classical SP fit (simple prediction fit). With simple prediction, the evaluated rate constants are slower than the real ones, as known from Farokhi et al. (2000). The results of the new approach (extended prediction fit) are much closer to the real values. However, at rate constants higher than 150 ms^{-1} the fitted rate constants start to exceed the real ones.

The "noise of the fit" gets obvious from the scatter in Fig. 3 as the curves are obtained from 250 independent fits with different rate constants. It is quite low for both kinds of approach in Fig. 3*A*, *B*. The start simplex includes the true rate constants, however, this is not of any relevance in the case of the prediction fit, because it is fairly independent of the starting values (*see*, for example left-hand side of Fig. 6).

However, the situation is not so good as may be suggested by Fig. 3*A* because these simulations are done with low noise, SNR = 10 (Eq. 1). Figure 3*C*, *D* shows the dependence for a $C-O$ model with $k_{CO} = 10$ ms^{-1} and $k_{OC} = 5$ ms^{-1}. It is obvious that under the conditions of Figs. 3*A*, *B*, (SNR > 8), the fit works quite well. However, the deviations become serious with SNR close to one. In contrast, the classical direct fit of the time series with simple prediction is quite insensitive to noise (The low rate constants are chosen because they are in the range where both fits do equally well at very good SNR).

The reason for the failure of the new approach at high noise levels seems to be quite obvious: often the noise pretends values close to I_Z, the value of the current on the slope of the filter (Fig. 1). The assignment of these values to I_Z gets a high weight via Eq. 4, and the assignments to the true full level gets low weights. In the classical SP fit, the noise has to shift by half a level to cause a false alarm, whereas in the new approach a quarter is enough.

Because of this high sensitivity to noise, it has to be stated that the extended prediction algorithm does not yield a tremendous improvement over the classical SP fit. If high temporal resolution is desired, patch-clamp recordings get very noisy. With a 50 kHz filter, the SNR (Eq. 1) is rarely better than 4, more often it is close to 2. Thus, it has to be concluded that this approach can be applied only to patch-clamp data with very good SNRs. With bad SNRs, the importance of the inclusion of filtered noise (Venkataramanan et al. 1998a, b, 2000) becomes obvious.

Beta Distributions of a 2-State Model

In Fig. 4, again a simple $C-O$ model is used for the comparison of the performance of the first-order Beta fit and the higher-order Beta fit with that of the SP fit. Figure 4*A* shows that the higher-order fit based on simulations reaches the same good results as the first-order fit of the data filtered by a first-order filter. The results are much better than those of the direct fit of the time series with simple prediction, but also better than those of the extended prediction algorithm (Fig. 3).

The noise test in Fig. 4*B* shows that the 4th-order Beta fit of a two-state model (Eq. 1) is reliable for signal-to-noise ratios down to about 2.

Application of the Beta Fit to a 5-State Model

In order to compare the direct fit of the time series with simple prediction (SP) and the Beta Fit with 4th-order filter (BF4), the 5-state model of Eq. 2 is used. The SP fit begins from start simplex 2 with $a = 0.5$ (*see* Appendix, Eq. A2), the Beta Fit from start simplex 1. Figure 5 shows the results. It is impressive that the SP fit does quite well at low and medium rate constants. Only at the fast rate constants k_{OG} and k_{GO}, the SP fit does not reach the original values. The SP fit has the advantage of being robust. Even though it underestimates the fast rate constants (Fig. 5*C*, *D*) it does so with high reproducibility. Many runs with different start simplices showed that it is quite independent of the starting conditions (*data not shown*).

The Beta fit is very successful when fitting the fast rate constants of the *C-O* model (Fig. 4). However, it fails completely when applied to the 5-state model

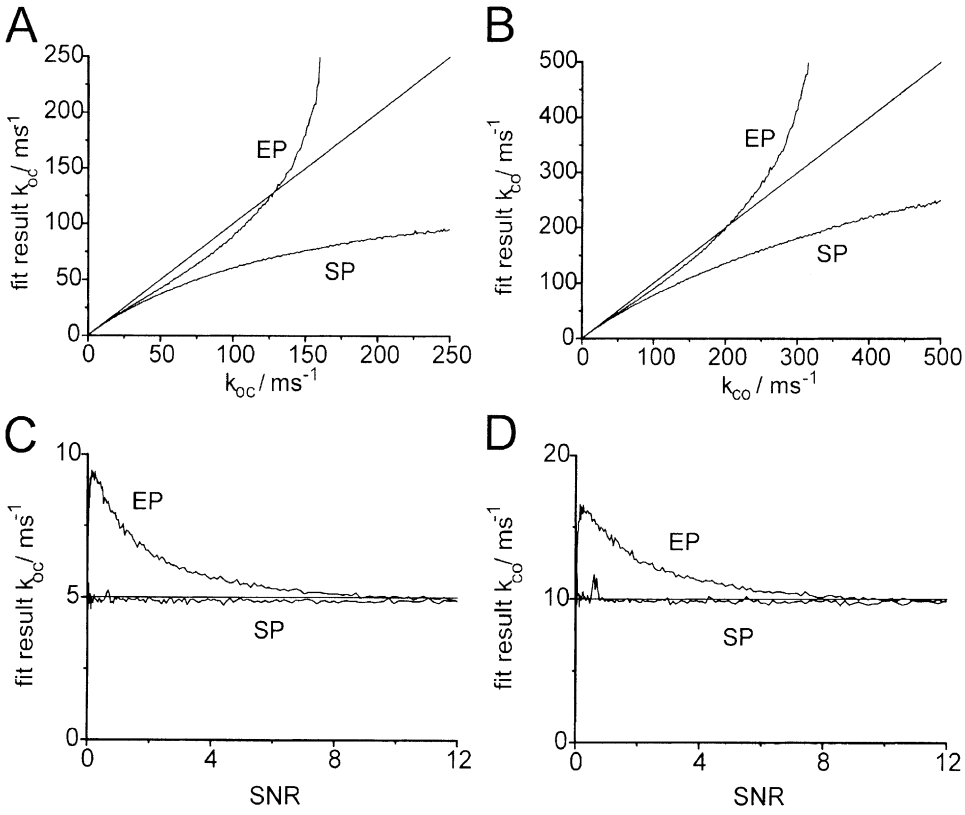

Fig. 3. Comparison of the performance of the direct fit of the time series with simple (*SP*, Eq. 3) and extended prediction (*EP*, Eq. 6) for a 1-channel 2-state model. The start simplex comprised the true rate constants ($a = 1$ in Eq. A2). The straight lines mark the correct results. (*A, B*) Range test with $k_{co} = 2\ k_{oc}$ *as given on* x-axis and SNR = 10. (*C, D*) Noise test with $k_{oc} = 5\ ms^{-1}$ and $k_{co} = 10\ ms^{-1}$.

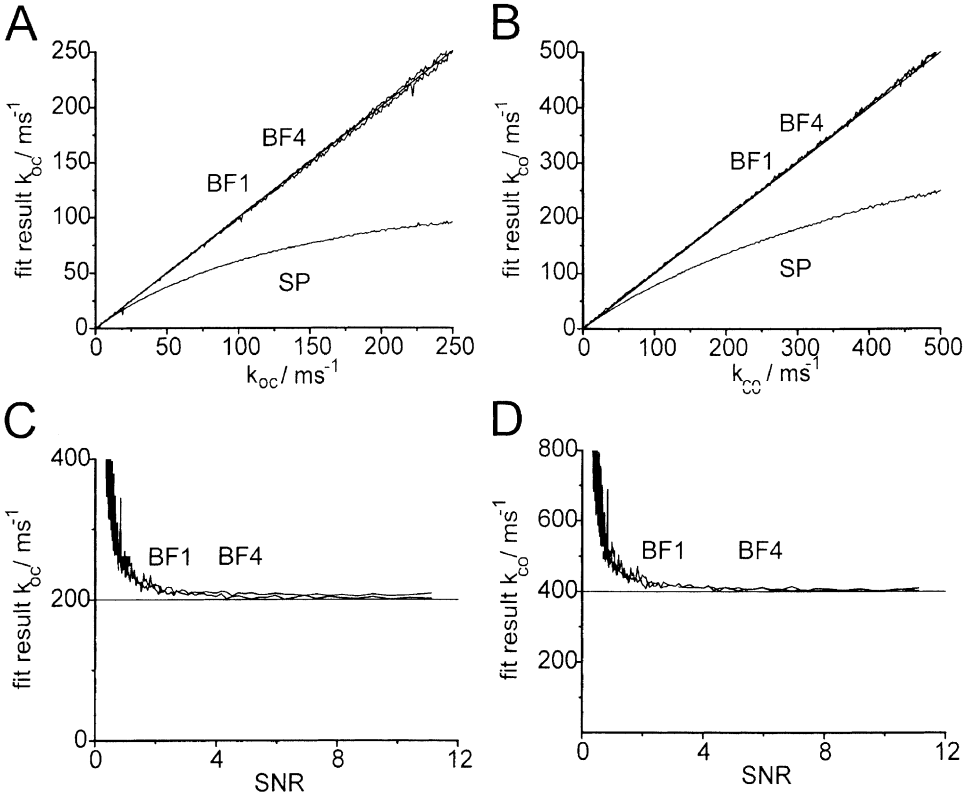

Fig. 4. Comparison of the performance of the Beta fits with first- and fourth-order filters (graphs not distinguishable) and the direct fit of the time series with simple prediction algorithm (SP) for a 1-channel 2-state model. The start simplex comprised the true rate constants ($a = 1$ in Eq. A2). The straight lines mark the correct results. (*A, B*) Range test with $k_{co} = 2\ k_{oc}$ *as given on* x-axis and SNR = 10. (*C, D*) Noise test for the Beta fits with $k_{oc} = 200\ ms^{-1}$ and $k_{co} = 400\ ms^{-1}$.

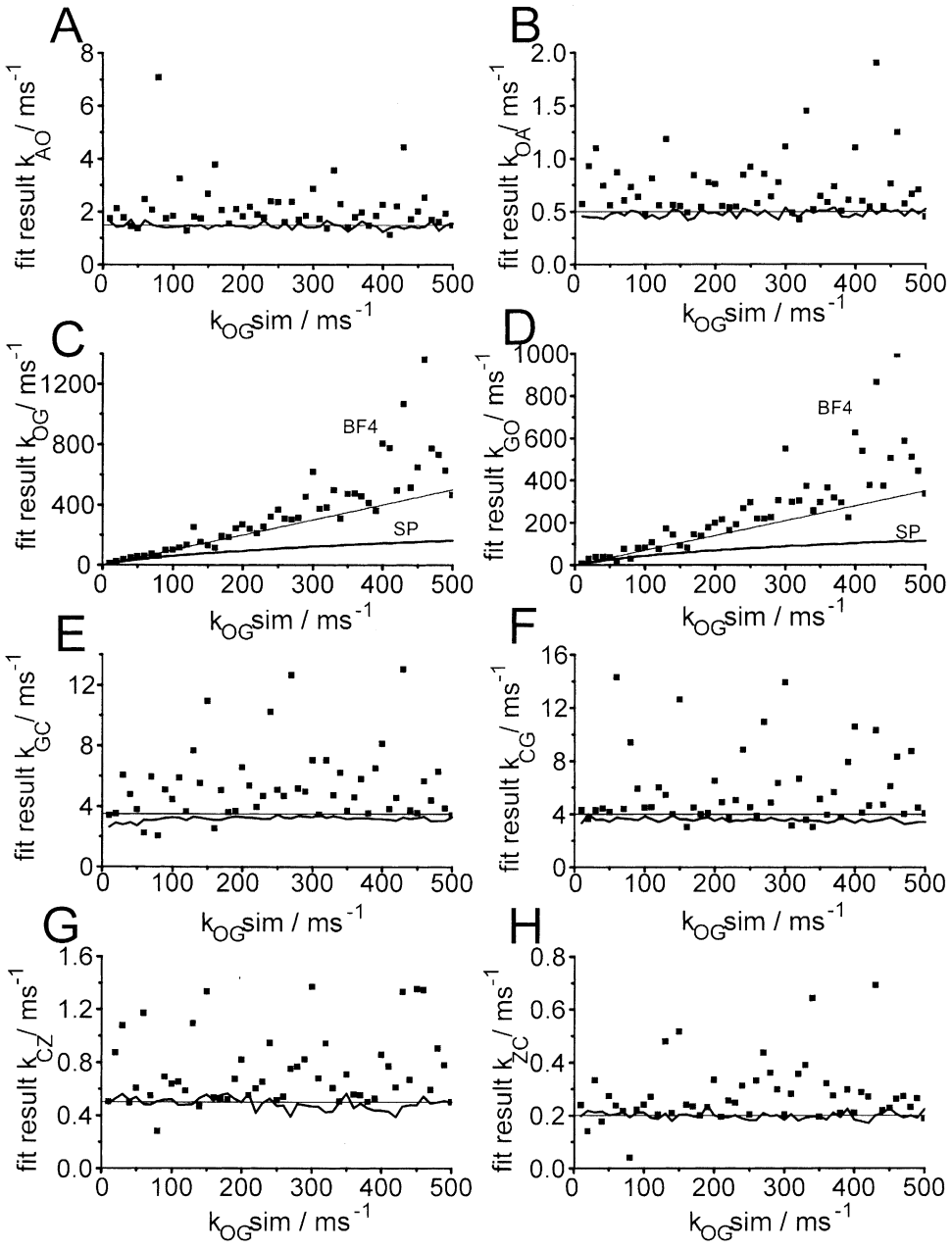

Fig. 5. Comparison of SP fit (*SP*) and Beta fit using the 5-state model of Eq. 2 by studying the influence of the fast rate constants 0.7 $k_{OG} = k_{GO}$ of the "measured" time series (given on the x-axis in all graphs) on the rate constants delivered by the fits. The straight lines give the true values (used for the simulation of the "measured" time series). The smooth lines present the result of the simple prediction SP fit (*SP*). The dots are obtained from a Beta fit with 4th order filter (BF4). In the case of the simple prediction fit, the start simplex (Eq. A1) is obtained with $w = 2$ and $a = 0.5$ (Eq. A2), and for the Beta fit it included the correct set ($a = 1$ in Eq. A2), and w in Eq. A1 is 10.

(Fig. 5) even if the start simplex includes the correct values ($a = 1$ in Eq. A2).

It is obvious that the slow rate constants cannot be determined by means of the Beta fit, because they do not cause a deviation from the gaussian shape of the amplitude histogram. However, a better performance could be expected for the fast rate constants k_{OG} and k_{GO}. But even though the slow rate constants do not influence the shape, they contribute to the steady-state occupancies of the states and consequently to the height of the amplitude distributions. Thus, an error in the slow rate constants may spoil the estimation of the fast rate constants.

Combining SP Fit and Beta Fit in a Simultaneous Fit

In order to combine the benefits of SP fit (high reliability at slow rate constants, high independence of fit performance on start simplex) with those of the Beta fit (correct fit of fast rate constants), a joint fit is done as described in the section New Approaches.

Figure 6 shows the dependence of the results of the simultaneous fit on the weighting factor g (Eq. 13). The results of the simultaneous fit are not encouraging. In the case of the slow transitions the joint fit inherits the high fit-scatter from the Beta fit. For the fast transitions, the rate constants increased monotonously with

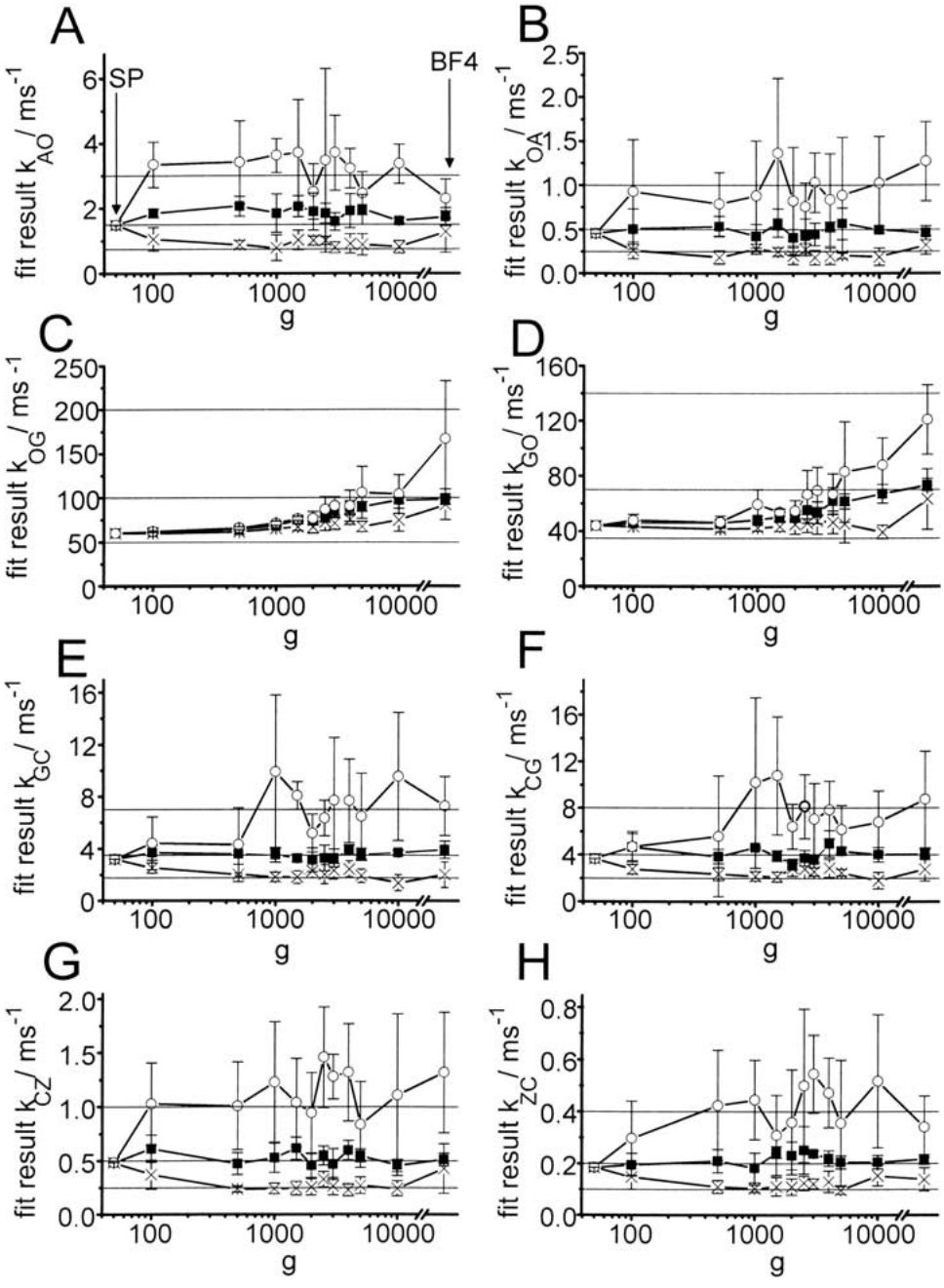

Fig. 6. Simultaneous fit of simple prediction fit and Beta fit. The dependence on the weighting factor g (Eq. 13) is tested for the 5-state model of Eq. 2 (averages of 5 runs) using three different start simplices (Eq. A2) with $a = 0.5$ (*empty circles*, upper horizontal line), 1 (*filled squares*, middle horizontal line) and 2 (*crosses*, lower horizontal line). The width w of the start simplex in Eq. A1 is 2 for the prediction fit and 10 for the Beta fit. The k_{ij} of the $s_{1,n}$ vertex (Eq. A2) of the start simplex are given as horizontal lines. The error bars resulted from 5 repetitions of the fits. The outermost left- and right-hand points result from the pure *SP* fit ($g = 0$) and from the Beta fit ($1/g = 0$), respectively, as indicated by the arrows in *A*.

g from the too low values of the pure SP fit ($g = 0$) to the higher and correct values of the amplitude fit (g very high). There is no reduction of the scatter of the fit by the incorporation of the SP fit.

It is to be mentioned that the pure SP fit (left-hand side of all graphs in Fig. 6) always finds the same parameters independently of the start simplex. The pure Beta fit is not successful (right-hand side of all graphs in Fig. 6) as already seen in Fig. 5.

The Beta fit is not capable of leaving the start simplex. The reason may be as follows: In one vertex $\{s_{1,n}\}$ of the start simplex the ratios of backward and forward reactions are already identical to the real values. This vertex already leads to occupations of the Markov states (and thus of relative heights in the amplitude histograms), which are already very good. All other vertices have random occupation probabilities and therefore produce worse amplitude histograms than $\{s_{1,n}\}$. This can prevent that the simplex of the Beta fit begins to crawl away from the start simplex. In Fig. 6, it can be seen that the fit results presented by crosses and open circles coincide with the horizontal lines representing $a = 0.5$ and $a = 2$ in Eq. A2, respectively. The SP fit, in contrast, puts more weight on the absolute values of the rate constants, and thus is not encaged by violations against

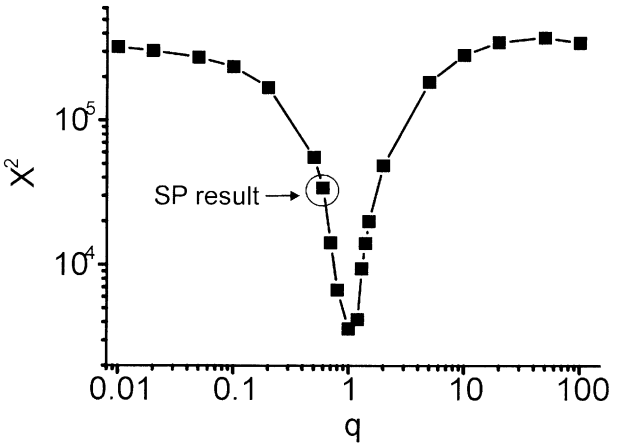

Fig. 7. One-dimensional error landscape for the Beta fit: The model of the "measured" time series is that of Eq. 2 with $k_{OG,0} = 300$ ms^{-1} and $k_{OG,0} = 210$ ms^{-1}. X^2 is calculated by means of Eq. 12 as a function of the deviation of the value of $k_{OG} = q\ k_{OG,0}$ and $k_{GO} = q\ k_{OG,0}$ from the true values ($q = 1$). The encircled point gives the X^2 for the value obtained from the SP fit.

the occupation probabilities. The important message of Fig. 6 is that the fitting performance cannot be improved by an adequate choice of the weighting factor g in Eq. 13.

Two-Step Approach of SP Fit and Beta Fit (SQ Fit)

The simultaneous fit above fails because SP fit and Beta fit have contradicting aims, in the case of the SP fit, the (too) low values of the fast rate constants yield the best criterion of fitness (maximum likelihood), and in the case of the Beta fit,the higher (correct) rate constants give the better criterion (minimum error). This conflict can be avoided by the subsequent approach: first, the SP fit is used to give a first estimate of the rate constants; then, the Beta fit is employed starting from these results.

In Fig. 7 the 5-state model of Eq. 2 with the fast rate constants being $k_{OG,0} = 300$ ms^{-1} and $k_{GO,0} = 210$ ms^{-1} is used to simulate the "measured" time series. Then, the "fitted" time series are obtained with $k_{OG,0} = q\ 300$ ms^{-1} and $k_{GO,0} = q\ 210$ ms^{-1} (q given at the x-axis in Fig. 7) and the error sum X^2 is calculated by means of Eq. 12. The result is very encouraging: Plotting X^2 over q shows that the solution of the SP fit is on the slope of the valley in Fig. 7, and that the best solution ($q = 1$) is at the bottom of the error valley. This shows that the error landscape of Beta fit provides optimum conditions for finding the "true" values.

Figure 8 shows a range test for the Subsequent-SP/Beta fit (SQ). The slow rate constants are not shown, as their behavior is that of the pure SP fit (Fig. 5). In Fig. 8, the SP fit shows the underestimation of the fast rate constants as already known from previous simulations (Figs. 3, 4, 6, 7). The results of the Beta fit are mainly found with the +/− 10% error range up to values of 500 ms^{-1}.

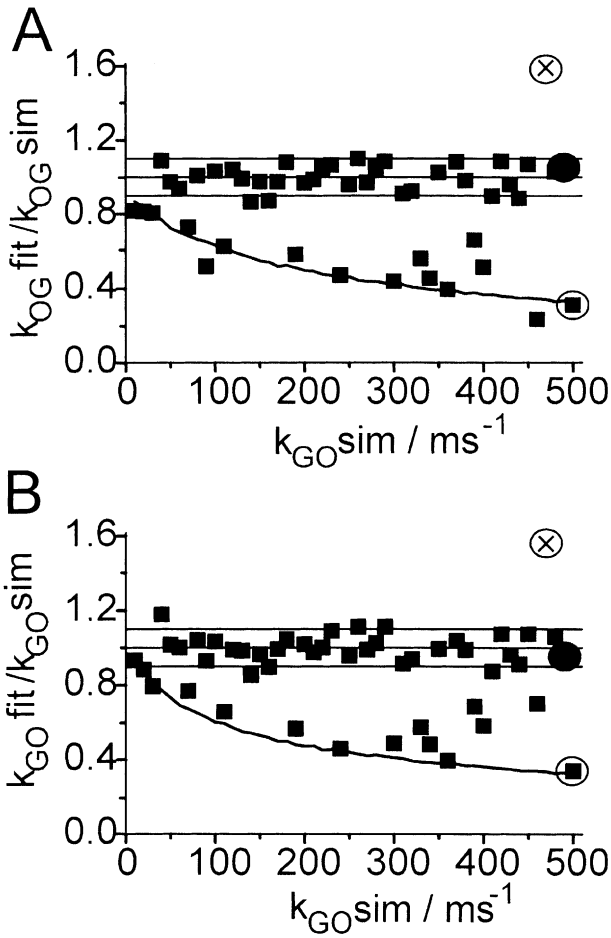

Fig. 8. Range test of the Subsequent SP/Beta fit. The middle horizontal line gives the true values and the parallel horizontal lines present 10% deviation.The descending curve presents the results of the SP fit. The *squares* show the results of the Subsequent SP/Beta fit. Start simplex was generated with $a = 0.5$ (Eq. A2) for the SP fit. The Subsequent Beta fit started from the fast rate constants of the SP fit with $a = 1$. In Fig. 9, the resulting amplitude histograms are shown for the three circled SQ results.

Not all Beta fits in Fig. 8 resulted in reliable k_{ij}, as becomes obvious from the points between the line presenting the SP fit and the horizontal lines giving the 10% error range around the true values. However, this is not a major problem, because the investigator has a simple means of detecting the failure of the fitting routine.

First, if the Beta fit does not move away from the result of the SP fit, the fit should be repeated. There is an important feature in Fig. 8, i.e., there are nearly no results of the Beta fit that are too high. If a fit is repeated those values of the rate constants that are higher are expected to be closer to the true ones.

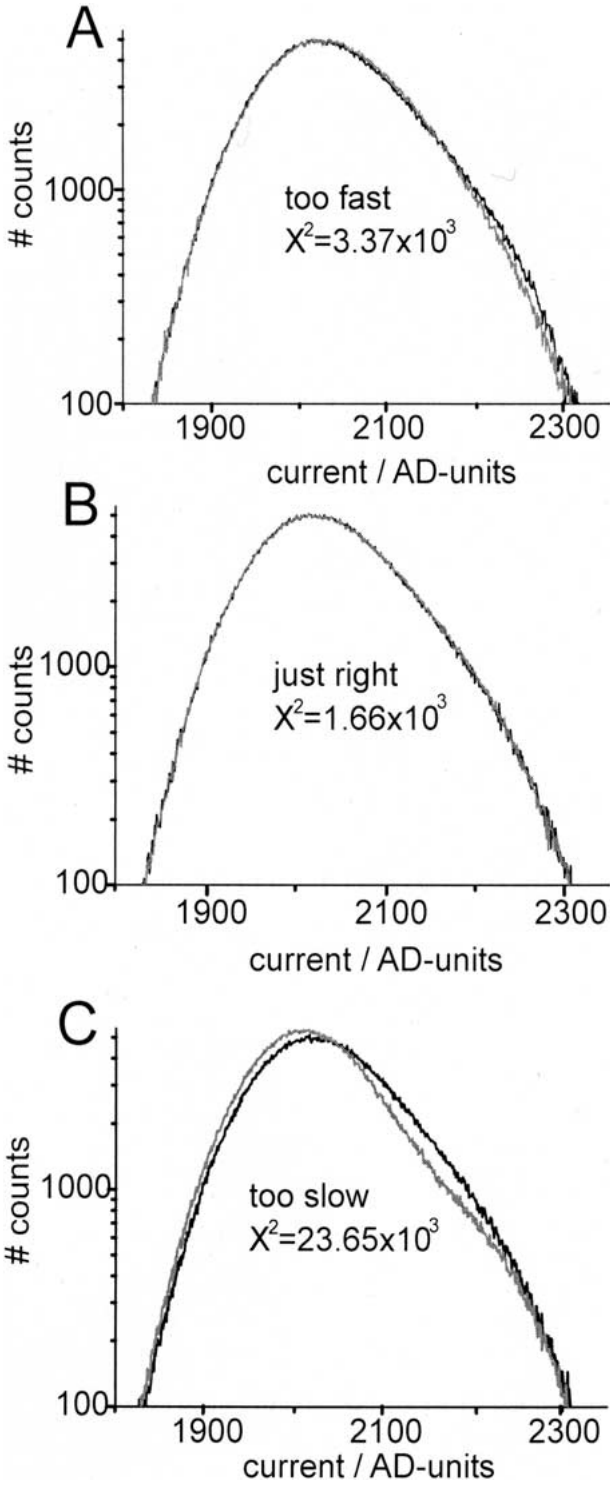

Fig. 9. Amplitude histograms as a means of detecting misfits in Fig. 8. The histograms belong to time series generated from a 5-state model (Eq. 2) with the slow k_{ij} of the SP fit and k_{OG} and k_{GO} improved by the Beta fit, which are (*A*) too large (*encircled cross* in Fig. 8), (*B*) correct (*filled circle*), and (*C*) too small (*encircled square*). The simulated time series is filtered by a fourth-order Bessel filter at 50 kHz.

Table 1. Computation time of some of the algorithms

	SP	BF4	SQ
1 Channel	10–20 min	10–20 min	15–25 min
2 Channels	60–90 min	10–20 min	60–100 min

The tests were performed on a Pentium 4 (2.5 GHz) under the following conditions: The duration of the simulated time series was 10^6 sampling points, and the start simplex was constructed as described above. The Markov model is given by Eq. 2 for $q = 30$.

Second, the related amplitude histograms of the Beta fits should be inspected. Figure 9*A*, *B*, *C* shows amplitude histograms calculated from the encircled values in Fig. 8. This is compared with the amplitude histogram obtained from a correct solution (*filled circle* in Fig. 8).

Figure 9*B* shows a perfect fit for the correct solution marked by the filled circle in Fig. 8*A*, *B*. The amplitude histograms in Figure 9*A* show a weak deviation for the rate constant that is too fast (*encircled cross* in Fig. 8*A*, *B*) and a more significant deviation in Fig. 9*C* for the rate constants that are too slow (*encircled square* in Fig. 8*A*, *B*). Even if the deviations are small in Fig. 9, they are an indication that the fit should be repeated. Figure 9 also shows that the sum of squares (X^2 given inside the histograms) can be used to distinguish the better solution from the less successful ones. Thus, the experimenter has a means at hand to check the reliability of the fit results.

Figure 10 shows the results of a noise test. It is evident that the SQ fit does well down to SNR of about 2. The low time constants determined by the pure SP fit are determined with sufficient accuracy, as already found in Fig. 5. The subsequent Beta fit also achieves that the fast rate constants k_{OG} and k_{GO} are determined with high accuracy. However, as already shown in Fig. 8, the scatter of the fit is serious. The absence of any monotonous correlation with the SNR shows that this scatter is of statistical origin related to the bad fitting performance of the Beta fit. As mentioned already when discussing Figs. 8 and 9, it is recommended to repeat the fit and use the comparison of amplitude histograms (Fig. 9) as a means of discarding misfits. The variability of repeated fits is introduced by the stochastic generation of the start simplex (Eq. A1) and the stochastic simulation of the time series.

Table 1 gives an estimate of the computing time for simulated data. Fitting a measured time series can take much longer, depending on the data quality. Especially, fits often have to be repeated several times. The random choice of the start simplex and the generation of the simulated time series of the amplitude histograms provide the chance to escape local extremes. The likelihood and the error of the ampli-

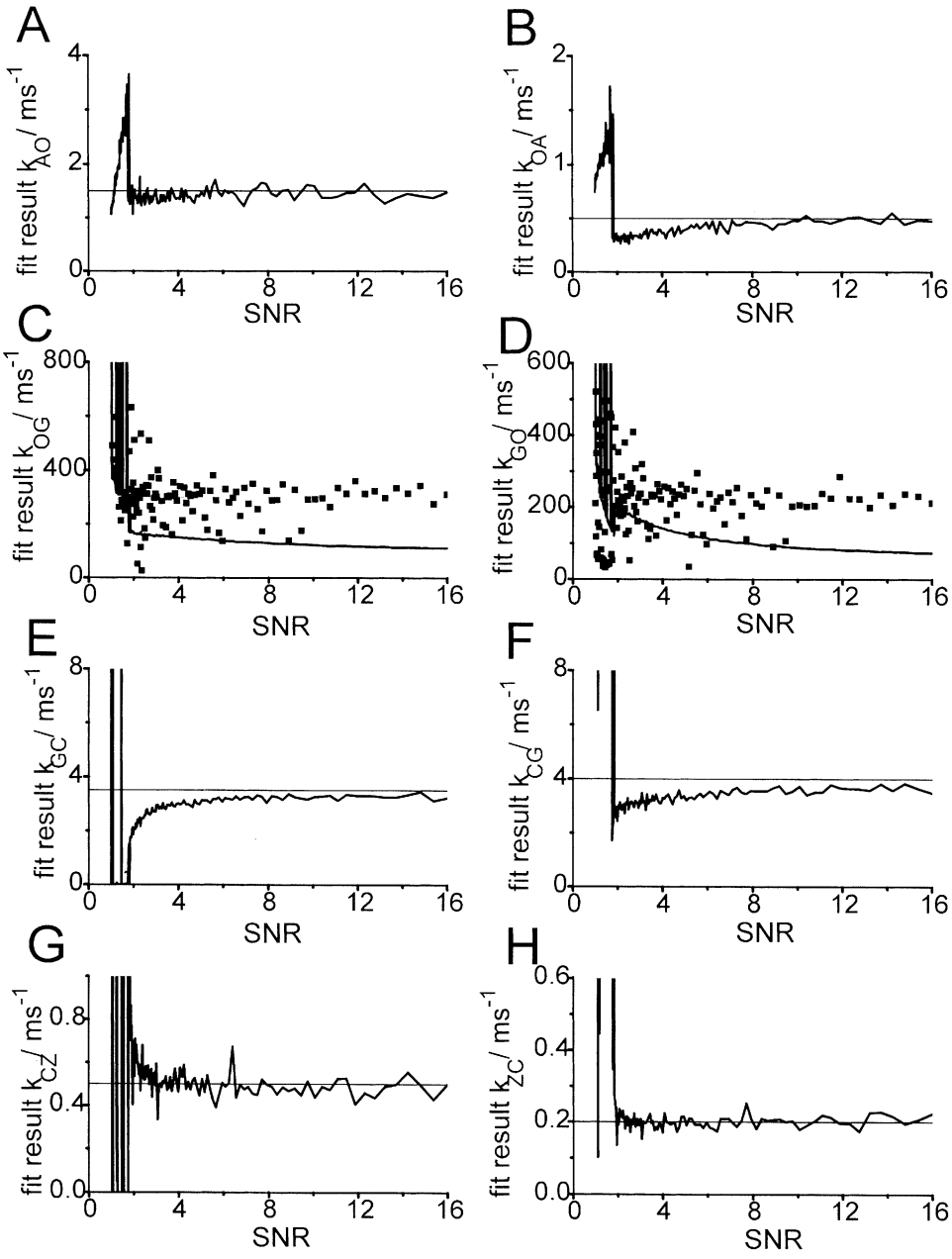

Fig. 10. Noise test of the Subsequent Beta/SP fit. The start simplex of the fit is obtained with $w = 2$ and $a = 0.5$ in Eqs. A1 and A2. The pure SP fit is given by the continuous line in most cases close to the true values (*horizontal line*). The Subsequent SP/Beta fit (*squares*) is restricted to the fast rate constants k_{OG} and k_{GO} (*C* and *D*).

tude histograms are used to select the best solution. For instance, a single SQ-fit from *Chara* (5 states, 2 channels, $2 \cdot 10^6$ data points) took about 4 h, and the solution shown in Fig. 11 was the best one out of ten.

Application to Real Data

The SQ fit is applied to patch-clamp data from *Chara*. Unfortunately, we have not been able to achieve 1- or 2-channel recordings. Thus, sections with only two channels open are cut out of the whole record and analyzed by the direct fit of the time series with simple prediction. It was already stated by Colquhoun and Hawkes (1982) that this procedure affects only the slow rate constants between shut states (in this case k_{CZ} and k_{ZC}). The SP fit resulted in the following rate constants

$$A \underset{28}{\overset{3.8}{\rightleftharpoons}} O \underset{41}{\overset{43}{\rightleftharpoons}} G \underset{2.8}{\overset{5.4}{\rightleftharpoons}} C \underset{0.2}{\overset{0.4}{\rightleftharpoons}} Z \tag{14}$$

(rate constants in ms^{-1}). From these rate constants a time series is simulated ($\sim 2.3 \cdot 10^6$ data points, same length as the measured time series), and the amplitude histogram for two channels is drawn. It is obvious that the amplitude histogram of the simulated time series (SP, *light gray curve* in Fig. 11) significantly deviates from the measured one (*black*

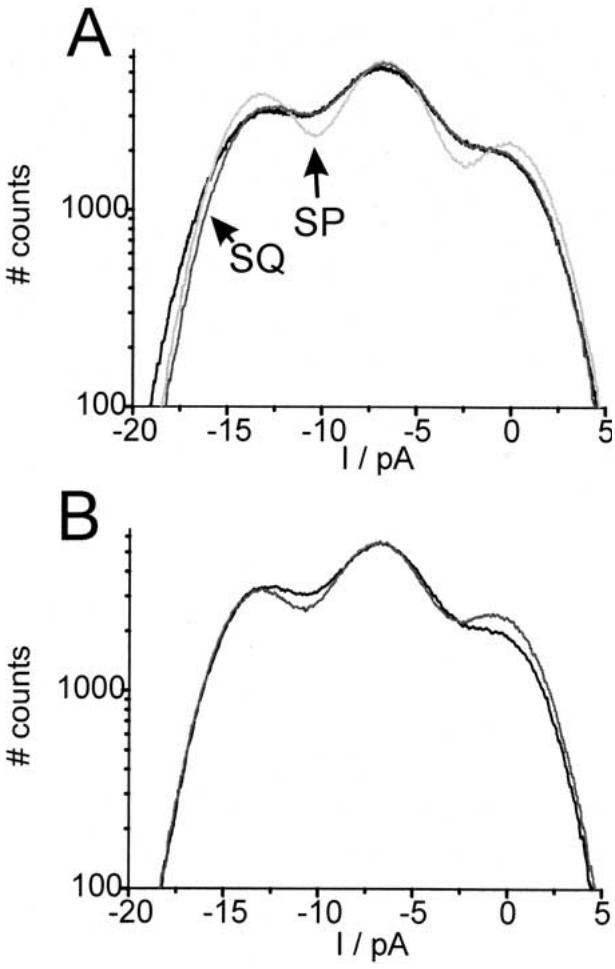

Fig. 11. (*A*) Comparison of the amplitude histograms obtained from time series generated from the results of the SP fit (*SP*) and of the subsequent Beta fit (*SQ*) of a 2-channel time series from *Chara*. The amplitude histogram of the experimental data is given by the black line. (*B*) Demonstration of the necessity of using three rate constants for the fit of the amplitude histogram of the model in Eq. 15. *Black curve*: Eq. 18 with the rate constants as given at the arrows. *Grey curve*: Eq. 18 with k_{OA} and k_{OG} being doubled.

curve). Now the subsequent Beta fit is performed. It used the slow rate constants as obtained by the SP fit. The fast rate constants k_{OA}, k_{OG} and k_{GO} are free. k_{OA} is not significantly modified by the subsequent Beta fit but k_{OG} and k_{GO} are strongly increased, leading to the improved Markov Model.

$$A \underset{28}{\overset{3.8}{\rightleftharpoons}} O \underset{939}{\overset{1000}{\rightleftharpoons}} G \underset{2.8}{\overset{5.4}{\rightleftharpoons}} C \underset{0.2}{\overset{0.4}{\rightleftharpoons}} Z \tag{15}$$

This set of rate constants results in a much better fit of the measured amplitude histogram (*SQ* curve in Fig. 11*A*). The resulting rate constants are quite high (k_{OG} = 1000 ms^{-1} and k_{GO} = 939 ms^{-1}). Thus, a time series with rate constants being half as fast as those resulting from the Beta fit is simulated. This doubles the deviation at the peak of the amplitude histogram, thus indicating that the transition rates between *O* and *G* are really in the range of 0.5 to 1 μs^{-1} (*data not shown*). These values are similar to those given by Schröder et al. (2004), which have been evaluated from distributions-per-level obtained from *Chara*.

It may be questioned whether it makes sense to use three free parameters in the amplitude fit. Simulations have shown that the SP fit may cause the following problem: a misfit of k_{OA} can be compensated by a misfit of k_{OG} in such a way that the relative occupation probabilities are preserved. Figure 11*B* shows the results of two simulations: the black curve is identical to the *SQ* curve in Fig. 11*A*. This is the best fit with the rate constants of Eq. 15. The grey curve in Fig. 11*B* is obtained also from the model in Eq. 15 but with k_{OA} and k_{OG} being doubled (this preserves the occupation probability of the open states). The difference in Fig. 11*B* is quite obvious and can be used by the fitting routine to distinguish the two parameter sets. Thus, all three rate constants have to be included in the amplitude fit in order to repair the failure of the *SP*-fit. However, it has to be mentioned that for values of k_{OA} below 30 000 the *SP*-fit alone has found the correct value. It has not been investigated whether it is a general rule that this limit is always close to half of the sampling frequency.

In contrast to the investigations with simulated data as used in Figs. 2 to 10, the fit of the measured amplitude histogram in Fig. 11 is not quite perfect. However, a better fit cannot be achieved on the basis of the employed 5-state model. The data shown are the best out of 30 fits, each taking about 3 to 5 hours because they were 2-channel fits. It has to be stated that real data are more complicated than simulated data.

In order to test the solution of the SQ fit a new time series is simulated with the rate constants of Eq. 15, using artificial white noise with the same σ as the measured time series. The SP fit of this time series results in

$$A \underset{28}{\overset{3.3}{\rightleftharpoons}} O \underset{138}{\overset{130}{\rightleftharpoons}} G \underset{3.6}{\overset{8.2}{\rightleftharpoons}} C \underset{0.5}{\overset{0.9}{\rightleftharpoons}} Z \tag{16}$$

(rate constants in ms^{-1}). The rate constants should be the same as those in Eq. 14. However, the values of k_{OG} and k_{GO} are twice as high. In a next attempt, a time series is generated from Eq. 15 as above, but the colored noise is taken from an obviously jump-free time series at 0 mV from the same patch. Using "real" noise changes the result of the SP fit of this time series to

$$A \underset{20}{\overset{3.8}{\rightleftharpoons}} O \underset{59}{\overset{43}{\rightleftharpoons}} G \underset{3.3}{\overset{6.6}{\rightleftharpoons}} C \underset{0.3}{\overset{0.7}{\rightleftharpoons}} Z \tag{17}$$

(rate constants in ms^{-1}). The rate constants of Eq. 17 are very close to those of Eq. 14. This leads to two

conclusions. First, the rate constants of Eq. 15 are the best estimates of those of the measured time series. Second, the choice of the correct noise is important. This stresses the importance of using filtered noise in the approach of Venkataramanan et al. 1998a,b; 2000).

Conclusion

Two basically different approaches have been tested to increase temporal resolution of the direct fit of the time series, one trying to improve the prediction algorithms of the SP fit (EP fit) with moderate increase of computing time, the other one combining the SP fit with the Beta fit (Subsequent SP/Beta fit). The simulations above show that inclusion of the filter response into the prediction algorithms of the direct fit of the time series can yield a higher temporal resolution. However, this holds only if the signal-to-noise ratio is excellent. This is a severe restriction for the application of this method, because in broadband recordings of patch-clamp current the SNR is usually worse than 4. Thus, it has to be concluded that the usage of filtered noise is a salient feature of the method of Venkataramanan et al. (1998a,b; 2000). This has stimulated the search for an alternative approach to account for filtering without increasing computing time too much.

In contrast to our expectations, the simultaneous fit of the time series and of beta distributions is not efficient. Obviously, it inherits only the faults of its parents, but not the benefits. This is probably caused by the fact that in the case of fast rate constants, SP fit and Beta fit are led by contradicting criteria of convergence to different optimum parameters sets.

Much more successful is the Subsequent SP/Beta fit. Even though the "theoretical" amplitude histograms have to be obtained from simulations of the time series for each iteration step in the curve fitting routine, the extra cost of computing time is still small compared to that required for the calculation of the Likelihood of the time series (Eq. 7). Figures 8, 10 and 11 show that a high temporal resolution far beyond the corner frequency of the anti-aliasing filter can be achieved even for 5-state models. Thus, this approach has the power to improve the temporal resolution of most of the patch-clamp recordings occurring in a real experiment.

Appendix

Generation of the Start Simplex

A simplex is a geometrical figure with $N+1$ corners (vertices) in an N-dimensional parameter space. The fitting routine starts from a start simplex, which has to be suggested by the investigator. Then it moves like an amoeba (Press et al., 1987) through the N-dimensional parameter space and searches for the optimum value of the convergence criterion.

The start simplex is generated as follows: A set of parameters $\{s_{1,n}\}$ is guessed by the experimenter. This set presents a point (vertex) in the N-dimensional space of the fit parameters with $n = 1...N$ being the index of the fit parameters, e.g., obtained from k_{ij} after arranging them in a sequential order. The simplex with $N+1$ vertices is generated as follows. The first vertex is $\{s_{1,n}\}$. Additional vertices ($s_{m,n}$ with $m = 2$ to $N+1$) are calculated from the following equation:

$$s_{m,n} = s_{1,n} \cdot w^{r} \tag{A1}$$

with w being the selected width of the start simplex and r a random number between -1 and 1. In section "Testing the algorithms", the vertex $s_{1,n}$ is obtained from the rate constants k_{ij} of the simulations

$$\{s_{1,n}\} = \{ak_{i,j}\} \tag{A2}$$

with the factor a being chosen by the experimenter as explained below. A width of $w = 2$ is used for the simple prediction fit, and $w = 10$ for the amplitude fit (Beta fit). The random number r has to be taken N^2 times from a random generator in order to generate the elements of the $N \times (N+1)$ matrix, which represents the $N+1$ vertices. This set of $N+1$ nondegenerate vertices is called the start simplex.

Simulation of Surrogate Time Series

Surrogate time series are used for two purposes. First, they are employed to generate simulated "measured" time series, which serve as examples for the application of the new tools. Second, they are required for the Beta fit to generate "theoretical" time series for the construction of "theoretical amplitude histograms". The basic approach of generating time series from a selected Markov model with an assumed set of states and rate constants has been described in previous papers (Blunck et al., 1998; Caliebe, Rösler & Hansen, 2002; Riessner et al., 2002, Schröder et al., 2004, program available at http://www.zbm.uni-kiel.de/software). Two random numbers are involved:

The first one ($n_1 \in [0,1]$) is used to calculate the time of the next jump (Δt) from the source state R_r to the sink (destination) state R_s in continuous time, with k_{rs}, k_{sr} being the rate constants of the transitions between R_s and R_r. It is obtained from the inversion of the dwell time distribution of the source state R_r

$$\Delta t = -\frac{1}{k_{rr}}\ln(n_1) \quad \text{with} \quad \sum_{s\neq r} k_{rs} = -k_{rr} \qquad (A3a, b)$$

s labels all possible sink states for a jump out of the present state R_r. The second random number n_2 (uniformly distributed, $0 \leq n_2 \leq 1$) gives the target of the jump (sink state R_s). The section between 0 and 1 is divided into sections of length $k_{rs}/-k_{rr}$ (Eq. A3*b*) assigned to the states R_s. The state R_s in whose section n_2 happens to fall is called the sink (destination) state. The system still remains in state R_r for the time Δt. Then, the jump to R_s occurs, and after this jump, the algorithm starts again from this new state by generating two new random numbers. It has been found that a length of 10^7 data-points is sufficient to keep the statistical variance of the "theoretical time series" small enough.

This time series is superimposed by white noise as defined by the selected signal-to-noise ratio (SNR)

$$SNR = \frac{\Delta I^2}{\sigma^2} \qquad (A4)$$

with ΔI being the single-channel current and σ^2 the variance of the noise. The resulting signal is fed into the same filter as used for the filtering of the experimental data.

In all simulations, the corner frequency of the anti-aliasing Bessel filter is 50 kHz and the sampling rate is 200 kHz, as commonly used in our group for the investigation of fast gating (Farokhi et al. 2000, Hansen et al. 2003).

This work was supported by the Deutsche Forschungsgemeinschaft Ha712/14-1,2. We are grateful to Enno Hammes for critical reading.

References

Albertsen, A., Hansen, U.P. 1994. Estimation of kinetic rate constants from multi-channel recordings by a direct fit of the time series. *Biophys. J.* **67:**1393–1403

Ball, F.G., Rice, J.A. 1992. Stochastic models for ion channels: introduction and bibliography. *Math. Biosci.* **112:**189–206

Ball, B.F., Yeo, G.F., Milne, R.K., Edeson, R.O., Madsen, B.W., Sansom, M.S.P. 1993. Single ion channel models incorporating aggregation and time interval omission. *Biophys. J.* **64:**357–367

Blunck, R., Kirst, U., Rießner, T., Hansen, U.P. 1998. How powerful is the dwell time analysis of multi-channel records? *J. Membrane Biol.* **165:**19–35

Caceci, M.S., Cacheris, W.P. 1984. Fitting curves to data - the simplex algorithm is the answer. *BYTE* **5/84:**340–362

Caliebe, A., Rösler, U., Hansen, U.P. 2002. A $\chi 2$ Test for model determination and sublevel detection in ion channel analysis. *J. Membrane Biol.* **185:**25–41

Colquhoun, D., Hawkes, A.G. 1977. Relaxation and fluctuations of membrane currents that flow through drug-operated channels. *Proc. R. Soc. Lond. B* **199:**231–262

Colquhoun, D., Hawkes, A.G. 1982. On the stochastic properties of bursts of single ion-channel openings and of clusters of bursts. *Phil. Trans. R. Soc. Lond. B* **300:**1–59

Colquhoun, D., Hawkes, A.G. 1990. Stochastic properties of ion channel openings and bursts in a membrane patch that contains two channels: evidence concerning the number of channels present when a record containing only single openings is observed. *Proc. Royal Soc. Lond. B* **240:**453–477

Colquhoun, D., Hawkes, A.G., Srodzinski, K. 1996. Joint distributions of apparent open times and shut times of single ion channels and the maximum likelihood fitting of mechanisms. *Phil. Trans. R. Soc. Lond. A* **354:**2555–2590

Csanády, L. 2000. Rapid kinetic analysis of multichannel records by a simultaneous fit to all dwell time histograms. *Biophys. J.* **78:**785–799

Draber, S., Schultze, R. 1994. Correction for missed events based on a realistic model of a detector. *Biophys. J.* **66:**191–202

Farokhi, A., Keunecke, M., Hansen, U.P. 2000. The anomalous mole fraction effect in *Chara*: Gating at the edge of temporal resolution. *Biophys. J.* **79:**3072–3082

Fredkin, D.R., Rice, J.A. 1992. Maximum likelihood estimation and identification directly from single-channel recordings. *Proc. Roy. Soc. Lond. B* **249:**125–132

Fredkin, D.R., Rice, J.A. 2001. Fast evaluation of the likelihood of an HMM: Ion channel currents with filtering and colored noise. *IEEE Trans Sig. Proc.* **49:**625–633

FitzHugh, R. 1983. Statistical properties of the asymmetric random telegraph signal with application to single channel analysis. *Mathem. Biosci.* **64:**75–89

Hansen, U.P., Cakan, O., Abshagen, M., Farokhi, A. 2003. Gating Models of the Anomalous Mole Fraction Effect of Single-Channel Current in *Chara*. *J. Membrane Biol* **192:**45–63

Hansen, U.P., Tittor, J., Gradmann, D. 1983. Interpretation of current-voltage relationships for "active" ion transport systems: II. Nonsteady-state reaction kinetic analysis of class I mechanisms with one slow time-constant. *J. Membrane Biol.* **75:**141–169

Jackson, M.B. 1997. Inversion of Markov processes to determine rate constants from single-channel data. *Biophys. J.* **73:**1382–1394

Kijima, S., Kijima, H. 1987. Statistical analysis of channel current from a membrane patch: II. A stochastic theory of a multichannel system in the steady-state. *J. theor. Biol.* **128:**435–455

Klein, S., Timmer, J., Honerkamp, J. 1997. Analysis of multichannel patch-clamp recordings by Hidden Markov models. *Biometrics* **53:**870–884

Klieber, H.G., Gradmann, D. 1993. Enzyme kinetics of the prime K^+ channel in the tonoplast of *Chara*: selectivity and inhibition. *J. Membrane Biol.* **132:**253–265

Korn, S.J., Horn, R. 1988. Statistical discrimination of fractal and Markov models of single-channel gating. *Biophys. J.* **54:**871–877

Magleby, K.L., Weiss, D.S. 1990. Estimating kinetic parameters for single channel using simulations. A general method which resolves the missed event problem and accounts for noise. *Biophys. J.* **58:**1411–1426

Michalek, S., Wagner, M., Timmer, J. 2000. A new approximate likelihood estimator for ARMA-filtered hidden Markov-models. *IEEE Trans. Sig. Proc.* **48:**1537–1547

Parzefall, F., Wilhelm, R., Heckmann, M., Dudel, J. 1998. Single channel currents at six microsecond resolution elicited by acethylcholine in mouse myoballs. *J. Physiol.* **512:**181–188

Press, W.H., Flannery, B.P., Teukolsky, S.A., Vetterling, W.T. 1987. Numerical Recipes. The Art of Scientific Computing. Cambridge University Press, Cambridge, New York, New Rochelle, Melbourne, Sidney,

Qin, F., Auerbach, A., Sachs, F. 2000. Hidden Markov modelling for single channel kinetics with filtering and correlated noise. *Biophys. J.* **79:**1928–1944

Riessner T. 1998. Level detection and extended beta distributions for the analysis of fast rate constants of Markov processes in sampled data. Ph.D. thesis, Kiel, Germany and Shaker-Verlag, Aachen

Riessner, T., Woelk, F., Abshagen, M., Hansen, U.P. 2002. A new level detector for ion channel analysis. *J. Membrane Biol.* **189:**105–118

Schröder, I., Huth, T., Suitchmezian, V., Jarosik, J., Schnell, S., Hansen, U.P. 2004. Distributions-per-level: A means of testing level detectors and models of patch-clamp data. *J. Membrane Biol.* **197:**49–58

Venkataramanan, L., Kuc, R., Sigworth, F. 1998a. Identification of hidden Markov models for ion channel currents - Part II: State-dependent excess noise. *IEEE Trans. Sig. Proc.* **46:**1916–1929

Venkataramanan, L., Walsh, J. L., Kuc, R., Sigworth, F. 1998b. Identification of hidden Markov models for ion channel currents - Part I: Colored background noise. *IEEE Trans. Sig. Proc.* **46:**1901–1915

Venkataramanan, L., Kuc, R., Sigworth, F. 2000. Identification of hidden Markov models for ion channel currents - Part III: Bandlimited sampled data. *IEEE Trans. Sig. Proc.* **48:**376–385

Venkataramanan, L., Sigworth, F. J. 2002. Applying hidden Markov models to the analysis of single ion channel activity. *Biophys. J.* **82:**1930–1942

Yellen, G. 1984. Ionic permeation and blockade in Ca^{2+}-activated K^+ channels of bovine chromaffin cells. *J. Gen. Physiol.* **84:**157–186

Yeo, G.F., Milne, R.K., Edeson, R.O., Madsen, B.W. 1988. Stastistical inference from single channel records: two state Markov model with limited time resolution. *Proc. R. Soc. Lond. B* **235:**63–94

Zheng, J., Venkataramanan, L., Sigworth, F.J. 2001. Hidden Markov model analysis of intermediate gating steps associated with the pore gate of Shaker potassium channels. *J. Gen. Physiol.* **118:**547–562